Tamjeed Journal of Healthcare Engineering and Science Technology E-ISSN: 2583-7281
Volume **1** (1): 2023, page 43-53, https://doi.org/10.59785/tjhest.v1i1.5 https://tamjed.com/

The Effect of Grain Size and Silicon Content on Non-Oriented Grain Steel Anomalous Loss Through Frequency Excitation in The Medical Healthcare by Using Big Data Analysis

Aiswarya RS[1]

[1]KPR Institute of Engineering and Technology, Coimbatore, India
Email: aishurs08@gmail.com

Veerandra Kumar R[2]

[2]Assistant Professor, Department of Computer Science and Engineering, Dhaanish Ahmed College of Engineering, Vanchuvancherry, Padappai, Chennai- 601301. India
E-mail: veerandrakumarr9@gmail.com

Punitha P[3]

[3]Assistant Professor, Department of CSE, SNS College of Technology, Coimbatore-641035, India
E-mail: punithapalanisamy93@gmail.com

Abstract

Using steels for commercial electromagnetic purposes produced by the Jordan Steel Group, the current research will look into the effects of grain size and excitation frequency on anomalous losses and the characteristics of the hysteresis curve of the anomalous loss. The final heat treatment of 21 steel samples for commercial electromagnetic purposes, divided into three groups differing in chemical composition, was carried out in the laboratory to determine the influence of electrical resistivity, grain size, and excitation frequency on total, hysteretic, and seek a better understanding of the effect of these variables on the anomalous loss portion. Compare the experimental data to the hypothesized constitutive equations in the literature and study to create the parasitic loss plus hysteretic loss curve using interpolation, superimpose it on the total loss hysteresis curve, then correlate the areas between the curves with anomalous loss and energy dissipation processes. It is possible to determine from micrographs and grain sizes that there was an increase in grain size due to normal brain development and a minor fraction of aberrant growth at high temperatures.

Keywords: Non-Oriented Grain Steel, Grain Size, Anomalous Loss, variables on the anomalous loss portion

Introduction

Electrical steel is the essential material among the magnetically soft materials and occupies the largest market share. In the case of silicon steels, Steels for magnetic purposes were developed in the late 19th century [1]. These steels correspond to 1% of the world's rolled steel production. In Jordan in 2020, it is estimated that the production of non-oriented grain steel was 352 thousand tons. The company, JSG Jordan steel manufacturing company estimates that in its new plant, the annual production of GNO steel will reach 400 thousand tons. The primary function of this material is to amplify magnetic induction due to its high magnetic permeability. They are sold in strips and coils for use in rotating core machines [2]. Part of the energy of electrical machines is dissipated when subjected to alternating electrical currents due to the generation of heat from the process of magnetization and associated demagnetization. The dissipated energy is associated with microstructural and dimensional factors. The energy dissipation rate is called iron power losses or magnetic losses. Due to the problems related to fossil fuels and the emergence of hybrid cars, the search for energy efficiency of electric motors is increasing. This fact drives the research and development of steels for electromagnetic purposes with low losses[3]. The separation of magnetic losses into three parts, hysteretic, parasitic and anomalous, becomes of paramount importance for understanding energy dissipation and manufacturing steels with greater energy efficiency. Among the parts that make up the total loss, this work focuses on the anomalous loss, considering that it is a function of the microstructure, electrical resistivity and excitation frequency [4].

Consequently, the abnormal loss is one of the most corrupt portions of energy at high frequencies. In the face of variables such as grain size, silicon content and frequency of excitation, there is no consensus among scholars regarding the weight of these factors. As a result, this research aims to study the relationship between particle size and excitation frequency in anomalous losses and the properties of the anomalous loss's hysteresis curve, utilizing commercial electromagnetic steels produced by the company Jordan Steel Group (JSG).

1.1 Classification of silicon steels for electromagnetic purposes: Siliceous steel is utilized to make electric motors and generators. In the quest for energy efficiency, silicon steels have progressively replaced non-alloyed steels. Silicon steels have a minimal loss due to their high electrical resistivity and microstructure [5]. The silicon steels used in electromagnetic applications are grain non-oriented (GNO) and grain-oriented (GO). GNO steels have no texture. The optimal texture for this steel in electric motors is cubic texture (100) [0vw], where the planes of the family [6] are randomly distributed on the surface of the sheet. The GNO has two subfamilies. GNO steel is fully treated without annealing. These steels have a thickness of 1 to 0.35mm, a silicon concentration of over 1.5% Si, and can be coated as JSG steels. Final annealing after stamping is required to regulate microstructural characteristics such as recrystallization, grain size growth, decarburization and residual stress [7]. Electrical equipment loses energy due to three factors: magnetic losses (iron losses), copper losses (eddy currents in conductors), and mechanical losses (friction). The loss of iron is the most important of the three factors responsible for energy dissipation. This amounts to around 45 billion dollars every year in the United States [8]. (10) [001] Grain-oriented steels are textured. They have a minimal loss and good permeability. Transformations, for example, require magnetic fields parallel to the longitudinal direction of the sheet, which these steels display due to their texture. Goss patented the GO manufacturing process in 1934, combining chemical composition, heat treatment, and cold rolling. The Goss texture is caused by atypical grain development [9].

1.2 The anomalous loss in GNO steels: Notably, non-oriented grain steel does not have a pronounced texture, so a complex domain structure exists in these materials. So the estimation of changes in the domain structure is very difficult to be performed. Such structure complexity complicates the treatment of anomalous loss for these steels. Bertotti (1985)[10] proposes the idea of magnetic objects, the “MO's”, translated as “magnetic objects”, are groups of coupled walls that cross grain boundaries, whose evolution in magnetization is strongly correlated, thus being able to be treated with a single region.

1.3 Grain size: Regarding the grain size, Lee et al. (2012)[11] showed the existence of an optimal grain size, which minimizes the total loss (Pt), as being 150 µm. From Figure 1, it is seen that the energy dissipation by eddy current (Pe) behaves linearly with the grain size. Pe corresponds to the sum of the parasitic loss and anomalous loss. As the parasitic loss is independent of the grain size, it is concluded that the effect is due to anomalous loss.

1.4 Anomalous loss and excitation frequency: Because the magnetic field changes direction when ferromagnetic material is magnetized at f, the domain walls must move quickly to compensate. The walls move faster as the excitation frequency increases, but the number of walls increases. To compensate for the minimal number of active walls, the velocity of the domain walls must be high at low excitation frequencies.

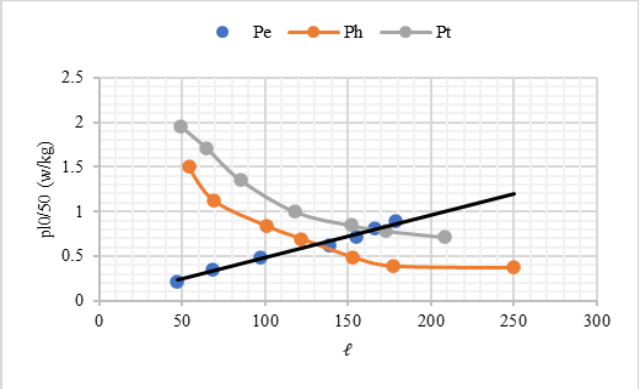

Figure 1: Influence of grain size on total (Pt) hysteretic (Ph) and most anomalous parasite (Pe) losses[12]

On continues to debate the impact of physical and microstructural factors on anomalous loss, as in Burak. (2017)[13]. Understanding how these variables affect losses is critical to reducing them and improving steel's energy efficiency for electromagnetic applications. Three steels with varying Si and Al concentrations were studied to determine whether Pa is proportionate to or inversely proportional to electrical resistivity. Doubts concerning the grain size effect warrant looking into the final temperature effect.

2.0 MATERIALS AND METHODS

To achieve the objectives proposed in this work, three alloys were used, composition given in Table 1, of GNO steels with 7 samples each alloy, in a total of 21 sets of Epstein blades with dimensions of 305 × 30 × 0.64 mm, cut in the longitudinal direction of the lamination. The silicon and aluminium contents were not strictly reported at the request of the materials manufacturer. The samples from each set were annealed at different final annealing temperatures, keeping the same temperature sequence for each alloy. Growth increased grain size by growth, thus producing different grain sizes in the samples.

Table 1- Chemical composition of alloys A1, A2 and A3.

Alloy No	samples	% of Si	% of Mn	Sulphur (ppm)	Carbon (ppm)	Titanium (ppm)	Nitrogen (ppm)
A1	36 to 42	2.05	0.42	30	20	25	26
A2	78 to 84	2.45	0.42	30	20	21	23
A3	120 to 126	3.3	0.55	8	28	20	22

2.1 Annealing

The annealing, pickling and cutting of the samples in the dimension 30x305mm were carried out at JSG. The annealing atmosphere, temperature and soaking time data are in Table 2, the three alloys were annealed in the same temperature sequence. The density and electrical resistivity of the alloys are listed in Table 3.

Table 2- Data related to annealing, temperature and atmosphere

samples			Final Temperarure recorded.°C	atmosphere Pressure	PO	Soaking time.
36	78	120	860	75% H_2 25% N_2	≤30°C	30 seconds
37	79	121	900			
38	80	122	940			
39	81	123	980			
40	82	124	1020			
41	83	125	1060			
42	84	126	1100			

Table 3- Resistivity and density

Alloy No	Density (2) Kg/m³	Resistivity (1) µΩcm
A1	7750	39.89
A2	7700	43.41
A3	7650	53.05

(1) Electrical resistivity measured at the EML; (2) Density provided by the manufacturer

2.2 Microstructural characterization

For the microstructural characterization of each sample, to determine the grain size, the test was performed according to ASTM E31[14-15]. The samples were cut and embedded; they were sanded in the 600 and 1200 MESH sequences through the polisher. Polishing was performed with diamond paste as an abrasive, with a granulometry up to 1µm and absolute ethyl alcohol as a lubricant. After polishing, the samples were etched with 10% Nital to reveal the grain boundaries. Subsequently, they were analyzed and photographed using the Olympus BX60M optical microscope as a coupled digital camera, model Opticam 5MP. Fourteen fields were randomly sampled, containing more than 30 grains each. According to ASTM E112[15], Grain size measurement was performed in Figure 2. Micrographs were taken at 100x magnification. Subsequently, they were opened in the ImageJ software (Image Processing and Analysis in Java), and through this, a circle of the known perimeter was superimposed. Thus, the intercepts were counted, emphasizing that intercepts that were tangent or point coming from the encounter of three grains had different counts, as determined by the ASTM standard. The average grain size was obtained by the ratio between the circumference of the circumference and the number of intercepts.

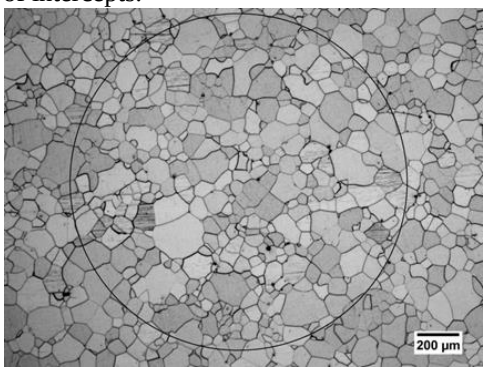

Figure 2: Micrograph is taken from the surface plane of the sample, GNO Fe-3.3%Si steel. Circle used for counting intercepts.

2.3 Essay on the Epstein board

The tests were carried out at the Electrical Metrology Laboratory – (EML). To determine the magnetic losses, the Epstein chart was used. This equipment consists of two windings and four coils connected in series for each winding; the primary is responsible for the excitation of the material and the secondary measures the flux density induced in it. The blades are introduced inside the winding forming a closed magnetic circuit. In this method, induction B varies with time. According to the ABNT –NBR 5161 [15] standard, the test was performed. Altogether, 21 sets of samples were tested, with 8 slides each, with an average weight of 0.4 kg in a frequency regime of 50, 60, 100, 150, and 200 Hz, 1 and 1.5T of induction, to determine the losses totals, here called Pt. The measurement of the hysteretic loss (Ph) was conducted in a quasi-static regime (0.005Hz) at 1 and 1.5 T. The hysteretic loss read on the device is the hysteretic loss value simulating conditions of use at 60 Hz. To convert this data into J/m³, multiply by density and divide by frequency. The analysis of the magnetic properties was carried out by the method of separation of losses, which considers the total loss as the sum of the parts that compose it, according to equation (1).

$$P_t = P_h + P_p + P_a \ldots\ldots (Eq.1)$$

3. Results and Discussion

3.1 Grain size and final annealing temperature

After heat treatment, all samples showed an increase in grain size by growth. The grain sizes (*P*), determined, and the temperature at which the samples were annealed.

The grain growth can be visually verified through Figure 3 (a,b,c), where the micrographs of the alloy three samples are shown. The micrographs were extracted from the annealed steels at temperatures of 900, 980 and 1100 °C. It is observed that there was normal grain growth and some abnormal growth, as some grains have more than 10 sides. It is also worth noting that the samples of alloy 1, annealed at the temperature of 1060 and 1100 °C, did not have grain growth; this fact is due to the phase change. The silicon content and the final annealing temperature allowed the austenitic transformation.

In Figure 4 the grain size evolution of alloys 1, 2 and 3 (A1, A2 and A3) are compared due to their sulfur content and grain size. At the final annealing temperature of 1100 °C, alloy 2 had the largest grain size. Alloy 2 has a lower concentration, in ppm, of titanium and nitrogen than alloy 1, as can be seen in Table 1. The sulfur concentration could justify the difference between grain size, in annealing at 1100 °C of alloys 1 and 3. In the hypothesis of the presence of manganese sulfide, it is plausible that it influenced grain growth. The grain boundaries can be anchored by manganese sulfide during grain growth, as highlighted in Zhang's (2013) work[16]. However, alloy 2 with 30ppm of S has a larger grain size at 1100 °C when compared to alloys 1 and 3, which makes a conclusive statement about this discrepancy inconsistent. It is also important to note that the final grain size is the result of some parameters such as: starting grain size and hot coil thickness.

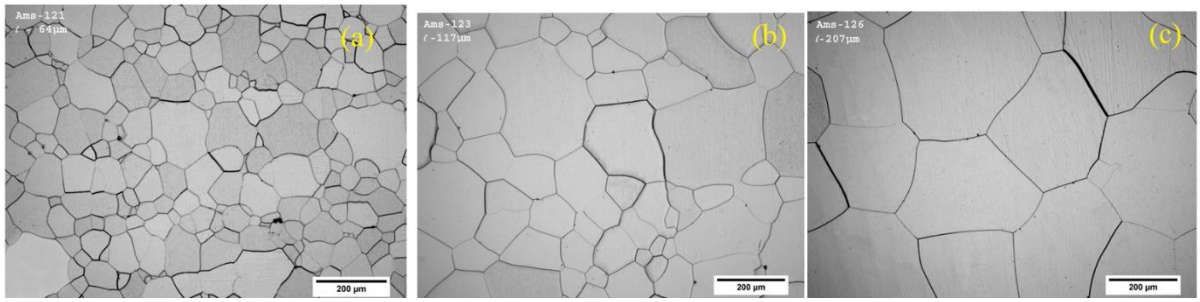

Figure 3: (a) Micrographs of sample 121 alloy 3, with 3.3%Si. We annealed at 900°C with a soaking time of 30 seconds, (b) Sample of 123 alloys 3, with 3.3%Si. Annealed at 980°C with a soak time of 30 seconds and (c) Sample of 126 alloys 3, with 3.3%Si and annealed at 1100°C with soaking time of 30 seconds, 100x magnification.

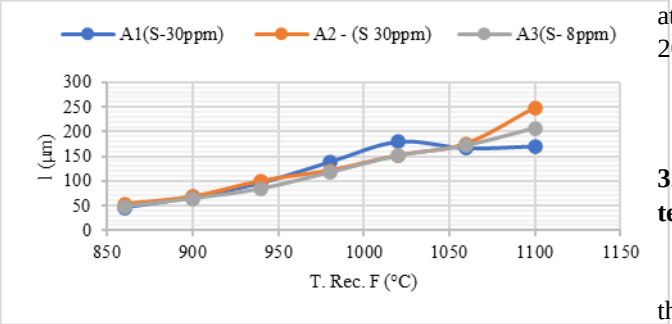

Figure 4: Grain size by final annealing temperature, comparison between alloys 1, 2 and 3, respectively.

3.2 Comparison between the measured magnetic losses of the EML and *JSG*

At *JSG*, the samples used in this work were subjected to the magnetic loss test at different frequency's for 1T and1.5T. In order to evaluate the reproducibility of the tests, the total loss measurements performed at the EML and *JSG* were compared. The result shows the percentage variation between the two measurements, *JSG* and EML, by the frequency at 1T. Results show the percentage change between the *JSG* and EML measurements of Pt by grain size ( ), with each sample's smallest and largest *P* of each sample. Both at 1 T and 1.5 T, the variations in total loss between the *JSG* and EML measurements did not exceed 4%. Note that the EML measures are generally smaller for the ratio (JSG/EML). The behavior of the results measured at frequencies from 50 to 2500 Hz at 1T is observed the occurrence of something abnormal in the measurements, above 500 Hz, and the anomalous loss becomes negative. This fact can be interpreted as if the parasitic loss calculated by equation (2) proposed by Thomson[17] added to the hysteretic loss, measured at 5 MHz, were greater than the total loss measured. However, this exposed error can be attributed to equation (2), as highlighted in (Zirka et al 2009)[18].

3.3 Magnetic losses, grain size and final annealing temperature

The loss treatment model applied in this work comprises the separation of the total loss into plots, according to equation (1), thus:

$$P_a = P_t + P_h + P_p \ldots\ldots (Eq\ .2)$$

As the grain size grew significantly with the annealing temperature and is a microstructural variable that has large effects on magnetic losses, it is important to evaluate the relationship between losses and grain size. Figure 5(a-c) shows the evolution of total loss as a function of annealing temperature at 60 Hz, with magnetic induction of 1.5 T, for the three alloys. Figures 5 (b) and (c) shows the particle size function (P_a), losses at 60 &150 Hz respectively, at 1.5T. It is generally observed that the anomalous loss increases with the increase in grain size. Only two cases deviate from the trend line: the annealing at 1100 ºC of alloys 1 and 3 resulted in lower anomalous losses than samples annealed at 1060 ºC of the same alloys. The anomalous loss is lower than expected for the *P*'s 178 and 207 µm of alloys 1 and 3, respectively. A hypothesis for the decrease of Pa with the increase of *P* can be based on the presence of nitrides; the content of N. Aluminum nitride (Al-N) can anchor the movement of domain walls. These residues are obstacles to the movement of the domain walls, so there will be dissipated energy for this obstacle to be overcome by the wall. The energy dissipated in this process will be increased to the hysteretic loss.

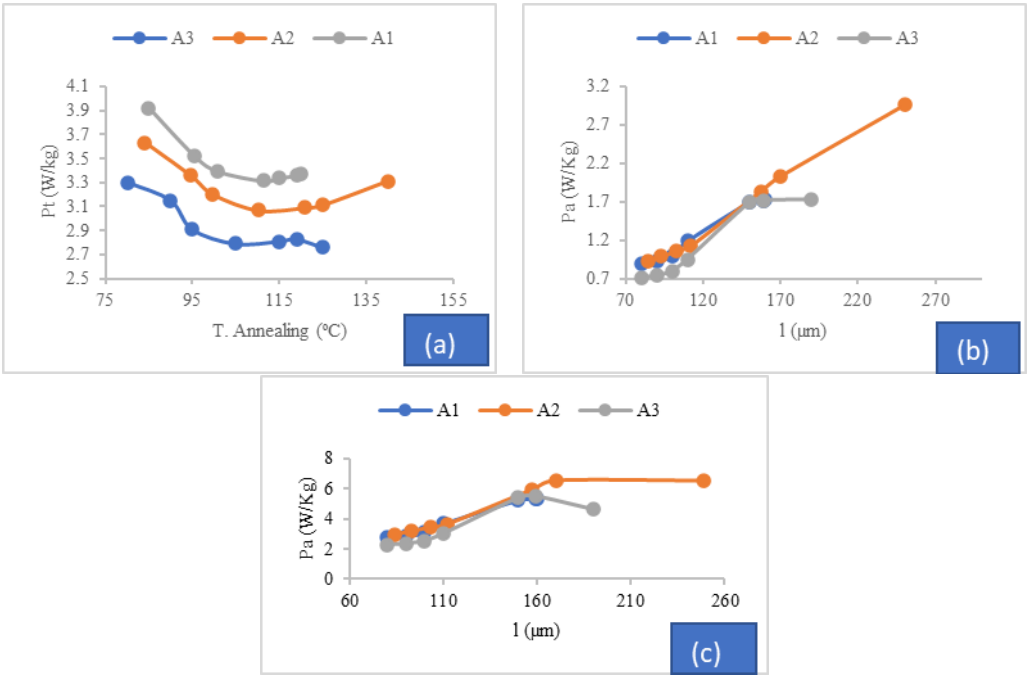

Figure 5. (a) Total losses by annealing temperature. Losses were measured at 60 Hz and 1.5T.; (b) Anomalous loss by *P*, comparison between alloys 1, 2 and 3 with their respective *P*'s, 1.5T at 60 Hz. Noticeable decrease in a loss in alloys 1 and 3 for *P* > than 175 µm; (c) Anomalous loss by *P*, comparison of alloy 1, 2 and 3 with their respective *P*'s, 1.5T at 150 Hz.

The hysteretic loss is expected to decrease with increasing grain size. It can be seen in Figure 6 that the Ph was increased only in the alloy 1 sample annealed at 1100 °C. Alloy 3 was expected to show an increase in hysteretic loss for the sample annealed at 1100 °C to compensate for the drop in Pa, however this did not occur. The increase in pH in alloy 1 of the sample annealed at 1100 °C can be explained by the hypothesis of the presence of Al-N, corroborating the study reviewed Nakayama in 2001[19]. However, the effect can also be attributed to the fact that samples annealed at temperatures of 1060 and 1100 °C have phase transformed. The decrease in grain size growth rate observed in Alloy 1 is reflected in the B50 measurement, as shown in Figure 6(b). The best B50 result for Alloy 1 corresponds to the sample annealed at 1060 °C.

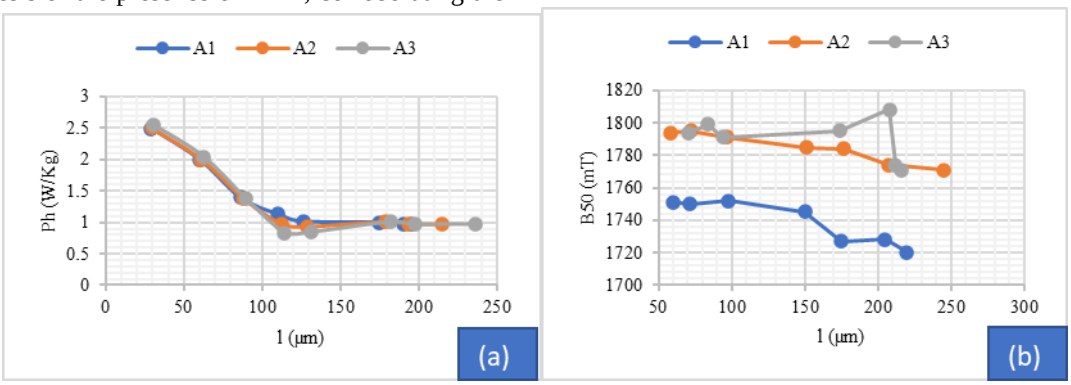

Figure 6: (a) Hysteretic loss by grain size alloy 1, 2 and 3, showing loss decreasing upon grain growth, loss increases with *P* > 175 µm of alloy 1, loss at 1.5 T. (b) Measurements of B50 in Alloys 1, 2 and 3.

3.3.1 Total losses, optimal excitation frequency and grain size

The total loss as a function of grain size, at 1 and 1.5 T and 50 Hz, is shown in Figure 7(a) with measurements from the EML and JSG and Figure 7(b), respectively. The figures show that the alloy 2 series clearly presented an optimal grain size, since this series goes from a maximum loss to a minimum and then grows again. This behaviour was evidenced in both EML and JSG measures. The optimal grain size for alloys 1 and 3 was chosen as *P* of lowest total loss, 154 and 207 µm respectively. There was a change in the optimal grain size (P_{oti}) with increasing induction, a behaviour corroborating the results of Lee et al (2014) [20].

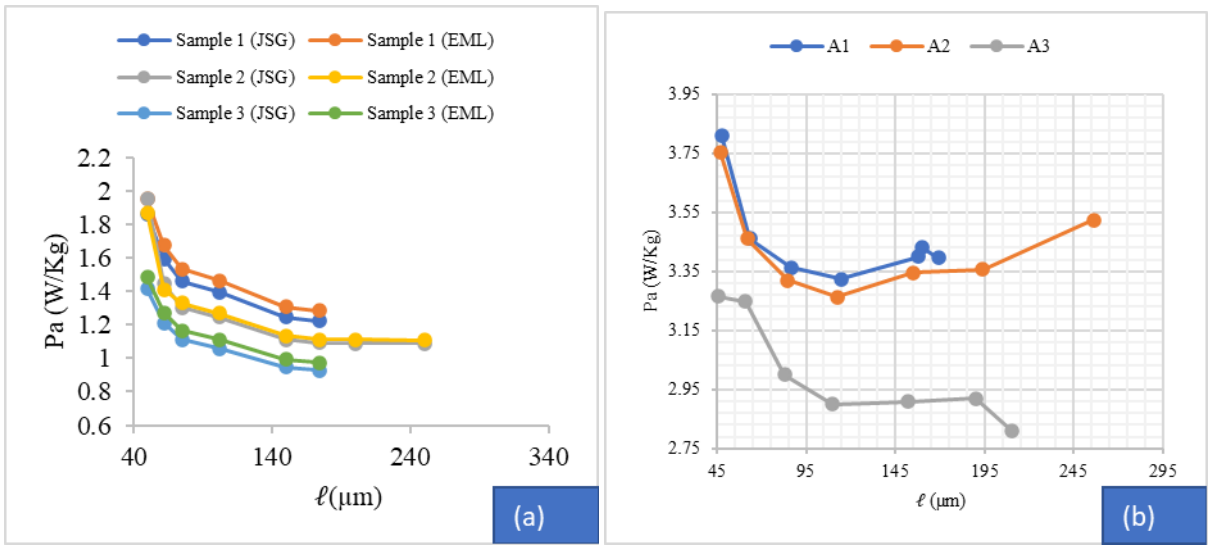

Figure 7: (a) Total loss and grain size, measured at 50 Hz at 1.0 T in EML and *JSG*, for alloys 1, 2 and 3. (b) At 1.5 T at EML, for alloys 1, 2 and 3.

3.4 Hysteretic losses and grain size

Hysteretic losses and grain size comparison and analysis results trend observed is very close to that of $P_h \; \alpha \; + \; \ell\sqrt{P}$ found in the literature[21]. Regarding the influence of grain size on hysteretic losses, it is highlighted that; the best behaviour was the loss growing with the inverse of the grain size with better R^2, the variation in the maximum induction did not modify this behavior. The results of $P_h \; \alpha \; \ell/P$ are in agreement with the results already highlighted in the literature [20]. The behaviour of hysteretic loss with the inverse of the grain size, as being linear, has been confirmed by other authors [21]. A hypothesis could be raised about the size of the inclusions. The sizes of the inclusion particles influence the hysteretic loss.

3.5 Hysteretic losses and the silicon content

Figure 8 shows the hysteretic loss at 1 and 1.5 T as a function of the silicon content for samples of the three alloys with similar grain sizes. Despite the imprecision of a three-point trend assessment, it is observed that the effect is very small if any. The energy dissipated in the hysteresis is approximately proportional to the energy of the domain walls, γ, which is proportional to $\sqrt{k1Tc}$. The addition of silicon reduces the saturation magnetic polarization, Js. Steel with added silicon has lower saturation, so it is expected that in a given induction, 1.5 Tesla, for example, this material is already close to saturation polarization. As the maximum induction affects the hysteretic energy according to Steinmetz's law, it is possible to propose that the effect of silicon on the dissipated energy is proportional to the saturation in the iron *Js*Fe divided by the saturation in the silicon steel *Js*Si. Combining the effect of Si on domain wall energy and saturation polarization, the relationship of equation (3) is proposed.

$$Wh \propto \left(\frac{J_{sFe}}{J_{sSi}(1 - a\%Si)}\right)^{1.6} \times \sqrt{K_1(1 - b\%Si)T_c(1 - c\%}$$

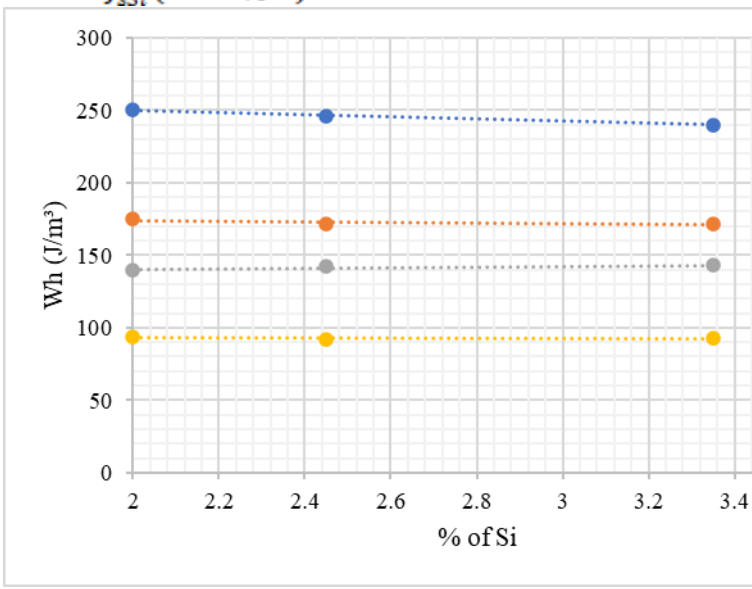

Figure 8: Hysteretic loss as a function of silicon content, comparison between alloys 1, 2 and 3, with close.

3.6 Loss due to anomaly as a function of grain size

For alloys 1 (2.05 %Si), 2 (2.45% Si), and 33.3% Si for 3rd alloy, the anomalous loss at 1.5 T was computed for frequencies of 50, 60, 100, and 150 Hz. The power trend line was used because it has the highest coefficient of determination R^2, indicating that the equation model better

explains the data. Equation (4) is the power equation used, where β is the pre-exponential factor and δ the exponent.

$$Pa = \beta \ell^{\delta} \quad \text{(Eq.4)}$$

From the graphs above, it can be seen that; the value of the exponent (δ) indicates the dependence of Pa on ℓ. The pre-exponential (β) is a function of the frequency for each sample, comparing the three alloys $\beta = f(f, \rho)$. Taking the average of the exponents for each league can be arranged as follows, and samples 1, 2 and 3 respectively. In Table 4 the coefficients of equation (4) are shown in more detail and the mean and standard deviation.

Table 4- coefficients of equation (4) for alloys 1 to 3, with Pa as a function of ℓ along with average coefficients of equation (1)

	Coefficients of Equation (4)			Average coefficients of equation (1)			
Alloy S.no	β	δ	f Hz	Mean (β)	SD (β)	Mean (δ)	SD (β)
A1	58.7	0.323	50	33.9545	9.971	0.32	0.009
	42.9	0.333	60				
	32.6	0.322	100				
	30.8	0.310	150				
A2	50.7	0.329	50	37.862	9.3391	0.35	0.018
	38.9	0.339	60				
	31.9	0.369	100				
	30.1	0.362	150				
A3	47.2	0.361	50	33.955	9.9706	0.34	0.022
	35.9	0.312	60				
	24.9	0.354	100				
	27.8	0.352	150				

For the three alloys studied in this work, the dependence of Pa on *P*, differs from the literature. Shinozaki (1989)[22] proposes that the eddy current loss is proportional to $\sqrt{\ell}$. In this case, the term "eddy current" is about the anomalous loss plus the parasitic loss, Pp not depending on ℓ. It is worth mentioning that the tests performed by the author were for total losses measured at 50 Hz. Matsumura (1984)[23] state that the eddy current loss is proportional to *P*, so Pa α ℓ. Returning to equation (4) it is notable that Pa α $\sqrt{\ell}^{2}$, by replacing the coercive field proportional to the inverse of the grain size. To highlight the difference between the influences of each grain size exponent on the anomalous loss, Figure 9 is taken as support. The three models are compared; Matsumura and Fukuda Pa α ℓ. (a), Shizaki Pa α $\sqrt{\ell}$ (b) and Pa α ℓ^{δ} (c), for δ average of 0.34, for alloy 2 at 60 Hz. Figure 9 compares the models Pa a $\sqrt{P}$ (a) and Pa a $P\delta$ (b), for δ mean of 0.34. Figure 9 compares the models Pa α $\sqrt{\ell}$ (a) and Pa α ℓ^{δ} (b), for δ mean of 0.34.

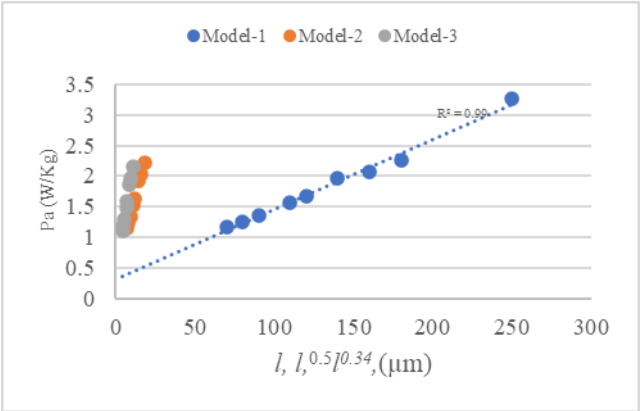

Figure 9: Anomalous loss by grain size, with the three exponent models and R² indicating the best exponent that describes the results. Turn on 2 with 2.45 %Si at 60 Hz.

From Figure 9 it can be seen that the best equation to describe the loss as a function of grain size was Pa α $\sqrt{\ell}$, when compared to the model Pa α ℓ. The linear relationship between grain size and anomalous loss can be seen in Figure 1; it is noted that the points are dispersed when compared with the hysteretic loss points of the same figure, this dispersion could indicate a non-linear relationship. By

comparing the losses with literature [10], it can be highlighted that, despite the dispersion, the largest R^2 obtained was for Pa a $P^{0.34}$. Another point to be observed in Figure 9 is the value of Pa, this very low value can be justified by the method of measuring the hysteretic loss. The data comparing the losses measured in [24] are data related to samples with different thicknesses. Different thicknesses lead to different Pp, hence a variation in Pa. However, R^2 is larger for the equation with an exponent of 0.34. It becomes evident that the R^2 that most closely matches the proposed equation is Pa $^{\alpha}P$0.5. They found average exponent of 0.34 can be expressed as a fraction, so 1/3. Therefore a dimensional analysis can be done in an attempt to establish a comparison between Pa α $\ell^{1/3}$ and the reference [24] Pa α $\ell^{1/2}$ Substituting the units of measurement into equation (5) we arrive at;

$$P_a = C_3 \ell^{\frac{1}{2}} \frac{1}{\rho} e^2 B_3^2 f^{1.5} (Eq.5)$$

$$P_a = C_3 m^{\frac{1}{2}} \frac{1}{\Omega \mathrm{m}} m^2 \left(\frac{Vs}{m^2}\right)^2 \frac{1}{s}^{1.5}$$

$$P_a = C_3 \frac{1}{\mathrm{m}^{\frac{5}{2}}} s^{-0.5} (Eq.5.1)$$

Where m is meter, s is second, Ω electrical resistance and V is volts. The same analysis with the exponent of 1/3, equation (5a);

$$P_a = C_3 \ell^{\frac{1}{2}} \frac{1}{\rho} e^2 B_3^2 f^{1.5} (Eq.5a)$$

$$P_a = C_3 m^{\frac{1}{3}} \frac{1}{\Omega \mathrm{m}} m^2 \left(\frac{Vs}{m^2}\right)^2 \frac{1}{s}^{1.5}$$

$$P_a = C_3 \frac{1}{\mathrm{m}^{\frac{8}{3}}} s^{-0.5} (Eq.5.2)$$

Comparing equations (5.1) and (5.2), it is noted that both are not dimensionally compatible. On the exponent of loss as a function of grain size, as 8/3 is closer to 3 than 5/2, we would have Watts per cubic meter in equation (5.2).

The physical meaning of anomalous losses, as a function of grain size, comes from the behavior of the domain walls in frequency. The anomalous is considered to grow with increasing grain size. Therefore larger grain sizes larger distances between domain walls. By subjecting the grain to frequency magnetization and demagnetization, there is an increase in the velocity of the domain walls, generating eddy currents. These currents are proportional to the velocity of the walls squared.

3.7 Anomalous losses and the excitation frequency

To analyze the anomalous loss as a function of frequency are taken. The power curve was used because it has the highest coefficient of determination R^2, indicating that the model of equation (6) explains the data variation.

$$P_a/f = Af^{\alpha} \ (Eq.6)$$

Where A is the pre-exponential factor and α power.

Mean and standard deviation of coefficients of equation (6), as a function of *P* for the three alloys, are allocated in Table 5.

Table 5 – Coefficients of equation (6) and the coefficient of determination R^2 as a function of *P*, Alloys 1 to 3 with different silicon concentrations and Mean and standard deviation of coefficients for each league.

Alloys 1 with 2.05%Si.				Alloys 2 with 2.45 %Si.				Alloys 3 with 3.3 %Si.			
P(µm)	A	α	R^2	*P*(µm)	A	α	R^2	*P*(µm)	A	α	R^2
47	8.010	0.650	0.9992	54	11.317	0.591	0.9989	49	7.654	0.640	1.000
68	9.468	0.638	0.9995	69	12.378	0.592	0.9989	65	8.796	0.640	0.998
97	10.884	0.646	0.9999	101	11.184	0.628	0.9997	85	8.457	0.655	0.999
139	12.322	0.662	1	122	11.449	0.650	0.9994	118	8.237	0.679	1.000
155	11.494	0.644	0.9993	153	13.559	0.640	0.9994	152	10.157	0.663	0.997
166	12.999	0.675	0.9999	177	14.265	0.643	0.9999	173	11.531	0.674	0.998
179	10.486	0.675	0.9999	250	15.890	0.628	0.9998	208	10.730	0.666	0.998

Sample Name	Coeffi cients.	Average	Std.Dev
A1	A	10.702	0.015
	α	0.649	
A2	A	12.736	0.024
	α	0.619	
A3	A	9.273	0.015
	α	0.653	

For each alloy the pre-exponential factor (A) is a function of the grain size, comparing the three alloys the factor is a function of *P* and resistivity. As can be seen, the exponents of anomalous loss as a function of frequency varied significantly among the three alloys. The alloy with the highest standard deviation was alloy 3, Table 5. This standard deviation reflects the slope of the curves.

The exponent obtained by the power curves as 0.64, equation (7), is the average value between the three alloys and is close to that proposed in the literature [10].

$$\frac{P_a}{f} \alpha f^{0.64} \ldots \left(\frac{J}{kg}\right) = P_a \alpha f^{0.64} \ldots \left(\frac{W}{kg}\right) \ldots (Eq.7)$$

In general, the anomalous loss is given in the literature [10] as being proportional to $f^{0.5}$, which does not differ much from the results presented in this work, $Pa \alpha f^{1.64}$. Results shows the comparison between the two exponents, for the sample with grain size of 53 and 249 µm from alloy 2. The R^2's are very close (0.999 and 0.997), however the highest coefficient of determination was for the exponent of 0.64 by the fact that it was extracted from the sample itself. The physical treatment given to the anomalous loss as a function of frequency is based on the quantity and distance between the domain walls. The amount of domain wall (Q), in a ferromagnetic sample, increases in the form $Q \alpha \sqrt{f}$ as highlighted in [69]. Thus, the distance between the walls (D) can be expected to decrease with increasing frequency in the form of $D \alpha 1/f^{0.5}$, as proposed in [44] replacing the relation in Bloor and Martin [37]equation, can be given in the form of equation (8),

$$P_a = C f^2 D \times (W/kg) \text{ (Eq.8)}$$

Where C represents the other variables and constants. Substituting $D \alpha 1/f^{0.5}$ into equation (8) the ratio of P_a to f is evident.

4. Conclusions

Through micrographs and grain sizes, it can be concluded that there was an increase in grain size due to normal grain growth and a small fraction of abnormal growth at high temperatures. The total losses measured at IPT, in general, are greater than those measured at JSG, however not exceeding 4% difference, both at 1.0 and 1.5 T. As expected, the anomalous loss increased with increasing grain size (*P*), except for samples annealed at 1100°C for alloys with silicon contents 2.05 and 3.3%Si. Hysteretic loss systematically decreased with increasing grain size. The study objective for the three alloys, is best described by a power law of the type, $Pa \alpha P^{0.34}$. It should be noted that, when comparing the exponent of 0.34 with the 0.5, proposed in the literature [25], the coefficients of determination (R^2) are very close. For the three alloys studied, the anomalous loss as a function of excitation frequency can be described as $Pa \alpha f^{1.64}$ where Pa is given in (W/kg). The exponent obtained is very close to that proposed in the literature, described as 1.5 [25]. By superimposing the hysteresis of the more hysteretic parasitic loss on the hysteresis of the total loss, it can be inferred that most anomalous loss occurs in regions associated with the movement of the domain walls. There is also participation of the phenomena of nucleation and annihilation of domains. Finally, it can be concluded that it is possible to represent the hysteresis of each of the components of the total loss.)

Data availability statement: The data underlying the results presented in the study are available within the manuscript.

Conflicts of Interest: The authors declare that they have no conflicts of interest regarding the publication of this paper.

Funding statement: The authors declare that no funding was received.

References

[1]. Fiorillo, Fausto & Bertotti, Giorgio & Appino, Carlo & Pasquale, M.. (2016). Soft Magnetic Materials. Wiley Encyclopedia of Electrical and Electronics Engineering. 10.1002/047134608X.W4504.pub2.

[2]. Gaoyuan Ouyang, Xi Chen, Yongfeng Liang, Chad Macziewski, Jun Cui, (2019,) Review of Fe-6.5 wt%Si high silicon steel—A promising soft magnetic material for sub-kHz application, Journal of Magnetism and Magnetic Materials, Volume 481, Pages 234-250,

[3]. Ouyang, Gaoyuan & Chen, Xi & Liang, Yongfeng & Macziewski, Chad & Cui, Jun. (2019). Review of Fe-6.5 wt%Si high silicon steel—A promising soft magnetic material for sub-kHz application. Journal of Magnetism and Magnetic Materials. 481. 10.1016/j.jmmm.2019.02.089.

[4]. Moses, Anthony. (2012). Energy-efficient electrical steels: Magnetic performance prediction and optimization. Scripta Materialia. 67. 560–565. 10.1016/j.scriptamat.2012.02.027.

[5]. Sidor, Jurij & Verbeken, Kim & Gomes, Edgar & Schneider, Juergen & Rodriguez-Calvillo, Pablo & Kestens, Leo. (2012). Through process texture evolution and magnetic properties of high Si non-oriented electrical steels. Materials Characterization. 71. 10.1016/j.matchar.2012.06.006.

[6]. Godec, Matjaz & Jenko, Monika. (2001). Texture investigation of electrical steels. Metalurgija -Sisak then Zagreb-. 40. 19-22.

[7]. Wang, H. & Huang, X. & Xiang, L. & Qiu, S. & Wang, J.. (2013). A new method to improve the

density of favorable textures in non-oriented electrical steels. Metalurgia International. 18. 9-14.

[8]. Kutscher, C. & Logan, J. & Coburn, Timothy. (2020). "Accelerating the US Clean Energy Transformation: Challenges and Solutions by Sector." Renewable and Sustainable Energy Institute, University of Colorado Boulder. Page 25

[9]. He, Kun & Wang, Li. (2016). A review of energy use and energy-efficient technologies for the iron and steel industry. Renewable and Sustainable Energy Reviews. 70. 10.1016/j.rser.2016.12.007.

[10]. Bertotti, G., Physical interpretation of eddy current losses in ferromagnetic materials. II. Analysis of experimental results. Journal of Applied Physics, 1985. 57(6): p. 2118-2126.

[11]. Lee, Jeong-Jong & Kim, Young-Kyoun & Rhyu, Se-Hyun & Jung, In-Soung & Chai, Seung-Hee & Hong, J.P.. (2012). Hysteresis Torque Analysis of Permanent Magnet Motors Using Preisach Model. IEEE Transactions on Magnetics - IEEE Trans Magn. 48. 935-938. 10.1109/TMAG.2011.2174435.

[12]. Wegayehu Enbeyle, Abdulsttar Abdullah Hamad, Ahmed S. Al-Obeidi, Solomon Abebaw, Assaye Belay, Admasu Markos, Lema Abate, Bizuwork Derebew, "Trend Analysis and Prediction on Water Consumption in Southwestern Ethiopia", Journal of Nanomaterials, vol. 2022, Article ID 3294954, 7 pages, 2022. https://doi.org/10.1155/2022/3294954.

[13]. Bal, Burak. (2017). A Study of Different Microstructural Effects on the Strain Hardening Behavior of Hadfield Steel. International journal of steel structures. 18. 10.1007/s13296-018-0302-9.

[14]. Mohammad, Khairul & Zainudin, E. S. & Sapuan, S. & Zahari, Nur & Ali, Aidy. (2013). Fatigue Life for Type 316L Stainless Steel under Cyclic Loading. Advanced Materials Research. 701. 77-81. 10.4028/www.scientific.net/AMR.701.77.

[15]. ASTM, Standard Guide for Preparation of Metallographic Specimens, in E3 2007, 2007: West Conshohocken. p. 12.

[16]. Zhang, J. M. & Xu, Ke-Wei & Zhang, M.-R. (2003). Theory of abnormal grain growth in thin films and analysis of energy anisotropy. Acta Physica Sinica - Chinese Edition-. 52. 10.7498/aps.52.1207.

[17]. Jassal, Anoop & Polinder, Henk & Ferreira, J.A.. (2012). Literature survey of eddy-current loss analysis in rotating electrical machines. Electric Power Applications, IET. 6. 743-752. 10.1049/iet-EPA.2011.0335.

[18]. Zirka, Sergey & Moroz, Y.I. & Marketos, Filippos & Moses, Anthony. (2010). Loss Separation in Nonoriented Electrical Steels. Magnetics, IEEE Transactions on. 46. 286 - 289. 10.1109/TMAG.2009.2032858.

[19]. Nakayama, Taisei & Honjou, Noriyuki & Minaga, Takashi & Yashiki, Hiroyoshi. (2001). Effects of manganese and sulfur contents and slab reheating temperatures on the magnetic properties of non-oriented semi-processed electrical steel sheet. Journal of Magnetism and Magnetic Materials. 234. 55-61. 10.1016/S0304-8853(01)00208-6.

[20]. Lee, K.M. & Park, S. & Huh, M. & Kim, Jae-Song & Engler, Olaf. (2014). Effect of texture and grain size on magnetic flux density and core loss in non-oriented electrical steel containing 3.15% Si. Journal of Magnetism and Magnetic Materials. 354. 10.1016/j.jmmm.2013.11.030.

[21]. Campos, M.F. & Teixeira, Julio & Landgraf, F. (2006). The optimum grain size for minimizing energy losses in iron. Journal of Magnetism and Magnetic Materials. 301. 94. 10.1016/j.jmmm.2005.06.014.

[22]. Shiozaki, M. and Y. Kurosaki, The effects of grain size on the magnetic properties of nonoriented electrical steel sheets. Journal of Materials Engineering, 1989. 11(1): p. 37-43.

[23]. Matsumura, K. and B. Fukuda, Recent developments of non-oriented electrical steel sheets. Magnetics, IEEE Transactions on, 1984. 20(5): p. 1533-1538.

[24]. Campos, M.F. & Yonamine, Taeko & Fukuhara, Marcos & Landgraf, F. & Achete, C. & Missell, Frank. (2006). Effect of Frequency on the Iron Losses of 0.5% and 1.5% Si Nonoriented Electrical Steels. Magnetics, IEEE Transactions on. 42. 2812 - 2814. 10.1109/TMAG.2006.879897.

[25]. G. Bertotti, GDS, A. Ferro Milone et F. Fiorillo, On the effect of grain size on magnetic losses of 3% non-oriented Si-F e. J. Phys. Colloques, 1985. 46: p. 3.